Biosensors and Bioelectronics 124–125 (2019) 75–81

Contents lists available at ScienceDirect

Biosensors and Bioelectronics

journal homepage: www.elsevier.com/locate/bios

Point-of-care-testing of α-amylase activity in human blood serum

Nilanjan Mandal[a], Mitradip Bhattacharjee[a], Arun Chattopadhyay[b], Dipankar Bandyopadhyay[a,c,*]

[a] Centre for Nanotechnology, Indian Institute of Technology Guwahati, Assam 781039, India
[b] Department of Chemistry, Indian Institute of Technology Guwahati, Assam 781039, India
[c] Department of Chemical Engineering, Indian Institute of Technology Guwahati, Assam 781039, India

ARTICLE INFO

Keywords:
α-amylase
Starch
Nanoparticles
Conducting polymer
Biosensor
Point-of-care-testing

ABSTRACT

Activity of α-amylase enzyme in human serum indicates the onset of pancreatitis, mumps, cancer, stress, and depression. Herein we design and develop a biosensor for the point-of-care-testing (POCT) of α-amylase concentration in serum. The biosensor is composed of a glass substrate coated with an electrically conducting polyaniline-emeraldine-salt (PANI-ES) film covered with starch-coated gold nanoparticles (SAuNPs). Addition of different dosage of α-amylase on the biosensor selectively depletes starch stabilized on the SAuNPs, which changes the electrical resistance of the sensor. The change in electrical resistance show a nearly linear correlation with the concentration of α-amylase in buffer, which helps the detection of unknown α-amylase activity in the blood serum. The biosensor responds in a specific manner owing to the use of selective enzymatic chemical reaction between α-amylase and starch. The pathways to SAuNP formation on PANI-ES, time-dependent starch digestion with α-amylase, and the subsequent variation in electrical response was characterized to uncover the sensing mechanism. The chloride ions and the AuNPs present catalyse the starch-amylase reaction on the PANI surface to enable a sensitive detection of α-amylase in serum (25 – 100 U/l) at a quick response time of ~60 s. Integration of the biosensor with the built-in sourcemeter and a real time display help an immediate presentation of α-amylase level in the serum, comparable to the clinically approved methodologies.

1. Introduction

Integrating the specialities of bio-processes, reaction engineering, and nanotechology in micro or nanoelectronic devices have become a hallmark in the design and the development of the next generation micro-electro-mechanical-systems (MEMS) targeting biomedical applications.(Bhattacharjee et al., 2016; Bhattacharya et al., 2007; Gogoi et al., 2011; Gogoi et al., 2012; Kricka, 2001; Kricka et al., 1993; Manz et al., 1990; Saliterman, 2006; Singh et al., 2014; Vo-Dinh and Cullum, 2000; Whitesides, 2006; Wu et al., 2012; Ferrari et al., 2006) In particular, the highly selective bio-reactions on the surface of nanoscale objects such as the nanoparticles have shown the potential to improve the efficiency of various detection techniques by enhancing the sensitivity and response time.(Ahn et al., 2004; Bashir, 2004; Grieshaber et al., 2008; Homola, 2008; Vo-Dinh and Cullum, 2000) In near future, the sensors empowered with the special features of the nano- and biotechnology are imagined to produce the rapid, reliable, portable, and easy to use point-of-care-testing (POCT) tools for the immediate detection of multifarious ailments.(Ahn et al., 2004; Bhattacharjee et al., 2017; Chin et al., 2007; Kricka, 2001; Sia and Kricka, 2008; Vo-Dinh and Cullum, 2000; Yager et al., 2008; Yager et al., 2006)

For example, it is well known that the concentration of the α-amylase in different body fluids such as blood, saliva or urine is an important indicator of a number of common ailments.(Wilkins, 2009) The rise or fall of this enzyme indicate the onset of pancreatitis, pancreatic cancer, mumps, stress or depression, toxaemia in pregnancy, and liver cirrhosis.(Anderson, 2002; González et al., 2002; He et al., 2000; Janowitz and Dreiling, 1959; Nater et al., 2005; Swaroop et al., 2004; Warshaw and Fuller, 1975; Wilkins, 2009) However, the presently available methodologies to evaluate the amount of this enzyme from different biological sources involve time-consuming and expensive multi-step processes.(Cosnier, 1999; Foo and Bais, 1998; van Staden and Mulaudzi, 2000) Further, expert view is also necessary for the detection and analysis. In this direction, the point-of-care diagnostic tools detecting the concentration of α-amylase with immediate electrical or optical response are perhaps the need of the hour.(Robles et al., 2011)

The enzyme α-amylase (endo-1,4-α-d-glucan glucanohydrolase, EC 3.2.1.1) is produced in pancreas and salivary glands to hydrolyse starch into simple sugars. The enzyme has been estimated during the blood serum examination to detect many important health disorders. (Zajoncová et al., 2004) Thus far, the spectrophotometric techniques

* Corresponding author at: Department of Chemical Engineering, Indian Institute of Technology Guwahati, Assam 781039, India.
E-mail address: dipban@iitg.ernet.in (D. Bandyopadhyay).

https://doi.org/10.1016/j.bios.2018.09.097
Received 28 July 2018; Received in revised form 26 September 2018; Accepted 29 September 2018
Available online 09 October 2018
0956-5663/

are the most reliable and accurate pathways to detect the activity of α-amylase in blood serum.(Chavez et al., 1990) However, the involvement of costly UV–Vis spectrophotometry for analysis restricts the applicability of this process in the POCT devices.(Chavez et al., 1990; Dutta et al., 2016; Shetty et al., 2011) Alternatively, the electrochemical methods,(Mahosenaho et al., 2010; Yamaguchi et al., 2005; Zajoncová et al., 2004) fluorometry,(Murayama et al., 2006; Zhang et al., 1990) isoelectric focusing,(Takeuchi et al., 1975) electrokinetic processes,(Watanabe et al., 1998) chromatography,(Battershell and Henry, 1990) weight based detections,(Gibbs et al., 2015; Sasaki et al., 2008) and immunological methods,(Svens et al., 1989) have also been employed for α-amylase estimation. A recent study has disclosed the development of a device suitable for the POC detection of α-amylase employing a paper substrate where the differential colorimetric signal generated with the variation in the α-amylase loading has been converted into electrical signal using light dependent resistor. (Bandyopadhyay et al., 2016; Dutta et al., 2016) A brief discussion and comparison about the methodologies to estimate α-amylase in the diverse body fluids has been summarized in the Table S1, Section (I), in Electronic Supporting Information (**ESI**) and discussed. The table suggests that, presently, an electrochemical POCT device for the rapid and accurate detection of α-amylase is yet to be available commercially in the market.

Herein we report the development of an electrochemical biosensor and a proof-of-concept prototype for the detection of α-amylase in human serum. The biosensor is composed of an electrically conducting polymer poly-aniline emeraldine salt (PANI-ES) thin film,(Malhotra, 2001; Singh et al., 2006; Tahir et al., 2005; Trojanowicz and Krawczyński vel Krawczyk, 1995; Wang and Mu, 1999) which is sparsely populated with starch-coated gold nanoparticles (SAuNPs) on the surface. The PANI-ES film acts as a base material for the electrical signal transport apart from acting as an immobilization matrix for the SAuNPs.(Mallick et al., 2006; Pandey and Mishra, 1988; Tamer et al., 2011) It is well known that α-amylase selectively catalyses the hydrolysis of starch into simple sugars. Thus, dispensing the solutions of α-amylase of different concentrations on the sensor depletes dissimilar amounts of the starch molecules coated the gold nanoparticles (AuNPs), which leads to the variation in the electrical resistance of the sensor. The change in the electrical resistance vary almost linearly with the concentration of α-amylase in phosphate buffer, which helps in the development of the calibration curve.

The pathway to SAuNP formation on the PANI-ES substrate, the time-dependent starch digestion with α-amylase, and the variation in the subsequent electrical response have also been characterized to uncover the details of the sensing mechanism. Involvement of chloride ions and AuNPs on the PANI-ES film offers a fast response time with a superior stability during the signal processing. A calibrated proof-of-concept prototype has also been developed for the fast (~60 s) detection of α-amylase level in human serum, which promises to be superior to the available clinically approved methodologies. The reported prototype has shown the potential evolve into a portable, easy-to-use, fast, reliable, economic, and biocompatible POCT diagnostic tool for the immediate detection of pancreatitis, cancer, stress, and depression.

2. Results and discussion

2.1. Sensor fabrication

The schematic illustration in the Fig. 1 shows the steps to fabricate the α-amylase biosensor. The materials and methods employed for the experiments are discussed in the Section (II) of the ESI. The non-conducting PANI-EB was synthesized following a standard protocol, as described in the experimental section. Thereafter, the film was coated on a glass substrate by drop-casting the PANI-EB solution, as shown in the Figs. 1**(A)** and 1**(B)**. Solubility of the non-conducting PANI-EB in the organic solvents helped in the drop-casting of the film. Since the conducting PANI-ES was sparingly soluble in most of the organic and inorganic solvents, we chose to cast the non-conducting PANI-EB film on the glass substrate. The FESEM image in the Fig. 1**(C)** shows the surface textures of the non-conducting PANI-EB thin film. After coating the PANI-EB film, a specified amount of the mixture of $HAuCl_4$ and starch was dispensed on the PANI-EB surface, as shown in the Fig. 1**(D)**. Consequently, reduction of gold (Au) present in $HAuCl_4$/starch solution on PANI-EB film formed AuNPs on the film surface.

The FESEM image in the Fig. 1**(E)** shows the surface textures of the conducting PANI-ES thin film coated with SAuNPs in which a few of them are marked on the image with an arrow. The starch in the solution mixture acted as the stabilizing agent before bonding on the AuNPs to form SAuNPs. Furthermore, the addition of the acidic solution (pH of 5.2 at 25 °C) of $HAuCl_4$/starch mixture on the surface of the PANI-EB infused the conductivity to the film because of the formation of the PANI-ES (Han et al., 2010; Wang et al., 2001; Li and Kaner, 2005). The change from PANI-EB to the conducting PANI-ES was indicated by the change of dark blue colour of the film into dark green. Following this, α-amylase solutions of different concentrations were dispensed on the biosensor and the change in the electrical resistance across the sensor was measured by connecting it with a commercially available source-meter, using the electrical contacts made with the conducting silver paste on the sensor (Fig. 1**(F)**).

2.2. Reaction mechanism

In Fig. 2, we propose a mechanism of SAuNP formation. It is well known that starch is a poly-hydroxylated macromolecule consisting of glucose units connected by glycoside bonds to form amylose and amylopectin chains (Fig. 2**(A)**). In the present situation, during the reaction, a part of the starch molecules formed glucose owing to the partial hydrolysis of the glycoside bonds. (Wang and Copeland, 2015; Wang et al., 2003) Importantly, the hydroxyl groups of starch facilitated electrostatic bonding with Au^{3+} ions before folding around them to form a helical structure of polysaccharide (Chairam et al., 2009; Imberty et al., 1988; Jenkins and Donald, 1995; Raveendran et al., 2003). In such a scenario, the aldehyde terminal of the glucose molecule reduced Au^{3+} ions to AuNPs while glucose was converted to gluconic acid (Fig. 2**(B)**, Castillo-López and Pal, 2014; Engelbrekt et al., 2009; Pasta et al., 2010).

Subsequently, a stable starch-AuNPs composite was formed because of the interaction between the –OH group of the starch with the AuNPs, (Fig. 2**(C)**, Engelbrekt et al., 2013; Katti et al., 2009; Tajammul Hussain et al., 2008) Further, while $HAuCl_4$ was reduced to produce SAuNPs particles, a large amount of HCl remained on the film matrix. The HCl in the polymer matrix protonated the non-conducting PANI-EB film to produce conducting PANI-ES film (Fig. 2**(D)**). The excess Cl^- left in the polymer matrix catalysed the amylase-starch reaction when the samples loaded with α-amylase was dispensed on the sensor.(Engelbrekt et al., 2013) Importantly, presence of the Cl^- ions led to an improved response time of the biosensor. (Bernfeld, 1955; Levitzki and Steer, 1974; Numao et al., 2002; Sky-Peck and Thuvasethakul, 1977; Walker and Hope, 1963)

2.3. Characterization of reactions and materials

Fig. 3 (A) shows the XRD plots of the PANI-EB film on glass substrate (curve in black) and PANI-ES film with SAuNPs deposited on the surface (curve with red). While the former curve did not show any peak corresponding to the AuNPs, the later shows the presence of peaks at 2θ = 38.35°, 44.31°, and 64.75° to confirm the presence of AuNPs on PANI-ES. (Pillalamarri et al., 2005; Sarma and Chattopadhyay, 2004; Zareh et al., 2011) The FTIR spectra in the Fig. 3**(B)** shows the peaks for PANI-EB (curve in green) and PANI-ES coated with SAuNPs (curve in blue). The FTIR analysis was performed after lifting of the targeted portions of the film from the glass substrate. The amount of sample and

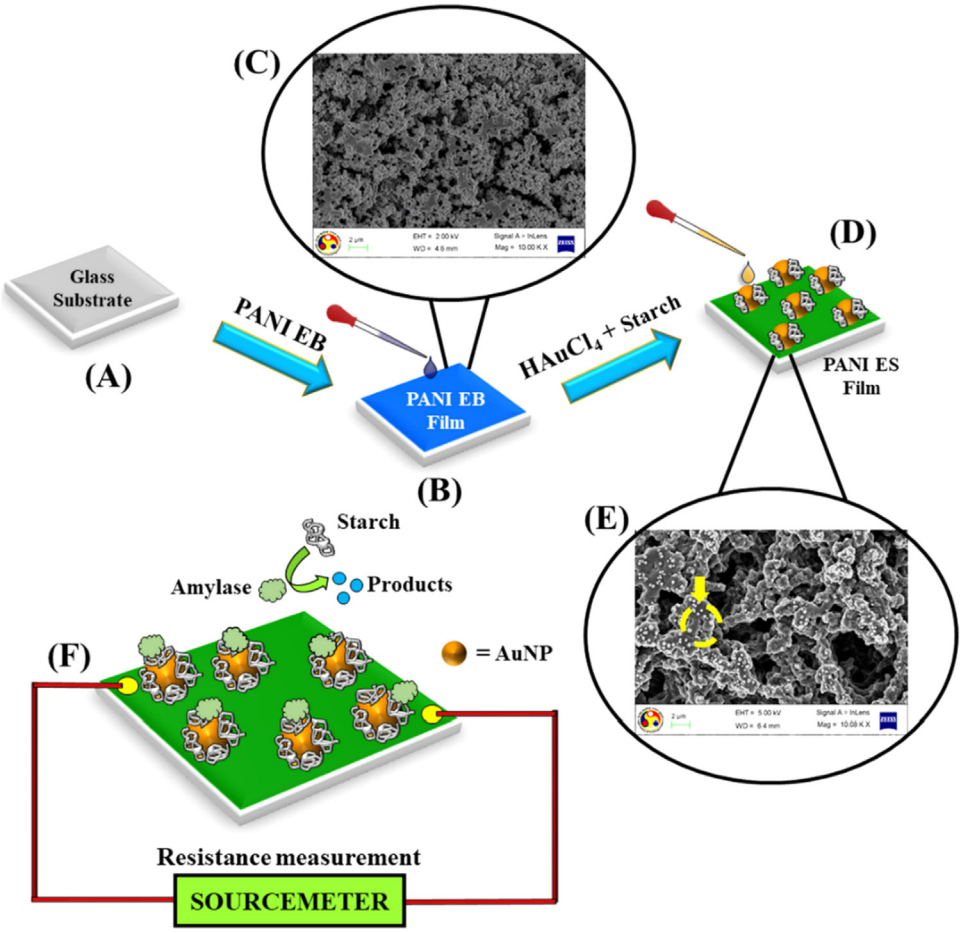

Fig. 1. Images (A) and (B) schematically show the coating of a PANI-EB film on a glass substrate. Image (C) shows the FESEM images of surface textures of PANI-EB film. Image (D) shows the formation of SAuNPs on the surface of the film and conversion of PANI-EB to PANI-ES. Image (E) shows the FESEM image of surface textures of the conducting PANI-ES film coated with SAuNPs, marked on the image with arrow. Image (F) illustrates the scheme for measurement of sensor resistance by sourcemeter.

KBr were kept constant. The characteristic peaks for starch were found at, 1022, 1079, 1156 cm^{-1}, and the region at 1200–1500 cm^{-1} (curve in blue). (Snabe and Petersen, 2002) The details of the peaks for PANI-EB (curve in green) and PANI-ES coated with SAuNPs (curve in blue) are provided in the Table S2 of Section (III) in the ESI.

Fig. 3**(B)** confirmed that the PANI-EB changed to PANI-ES due to protonation by the acidic $HAuCl_4$/starch solution. The starch shows bands at 3424 cm^{-1} corresponding to the stretching frequency of –OH group. Other absorption bands at 1652 cm^{-1} and 1411 cm^{-1} (curve in blue) are due to C–C and C–O stretching vibrations, respectively. The IR

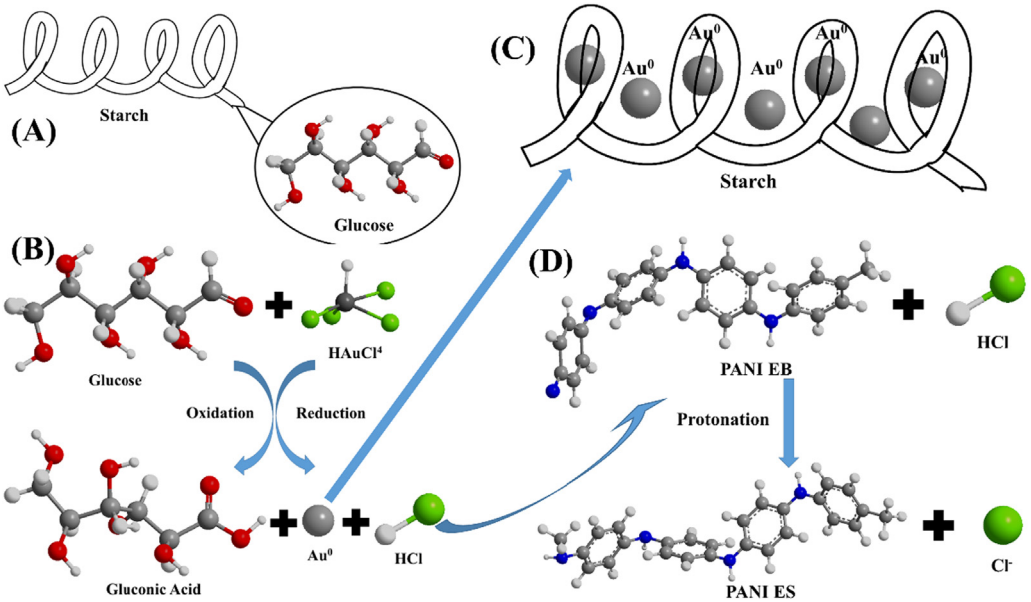

Fig. 2. Image (A) shows starch consisting of glucose units. Image (B) shows the reduction of the $HAuCl_4$ by glucose to form AuNPs. Image (C) shows formation of SAuNPs and image (D) shows the conversion of PANI-EB to PANI-ES by HCl alongside having Cl^- on the film matrix.

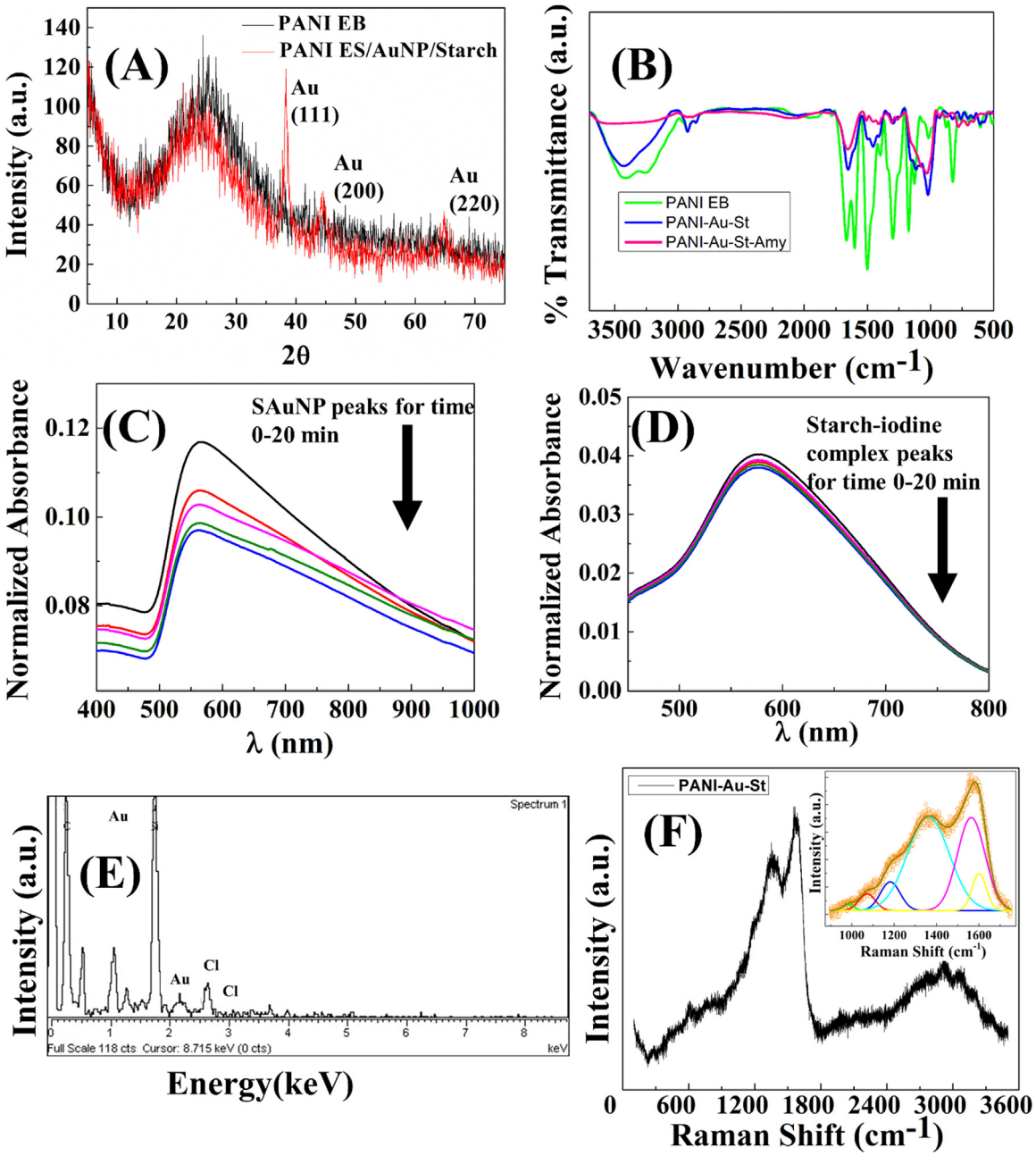

Fig. 3. The XRD plots in the image (A) correspond to the PANI-EB (darker – black) and PANI-ES coated with SAuNPs (lighter – red). The plot (B) shows the IR spectra of the sensor. The image (C) shows the UV–vis spectroscopy of α-amylase treated SAuNP composite at different time intervals, 0 min, 5 min, 10 min, 15 min, and 20 min, of starch digestion. The image (D) shows the UV–vis spectra of starch-iodine complex at the same time intervals of digestion of bare starch. Image (E) shows the EDXS plot of the sensor surface depicting the elemental composition. Image (F) shows the Raman spectra of the sensor surface whereas the inset shows the peak fitting for 900–1760 cm^{-1}.

analysis also provided further clues of SAuNP formation on PANI-ES. For example, the plots also indicate the formation of the SAuNP composite because of the interaction of the –OH group of starch molecules with the AuNPs on the PANI-ES surface following the mechanism discussed previously in the Fig. 2 (Engelbrekt et al., 2013; Katti et al., 2009; Tajammul Hussain et al., 2008).

Further, the curve in pink in the Fig. 3**(B)** shows the FTIR spectra of PANI-ES coated with SAuNPs after the reaction with α-amylase. The change in the characteristic peaks suggested the digestion of starch on the surface of the AuNPs, which might have led to the reduction in the electrical resistance of the sensor. (Deka et al., 2008) In order to further prove the aforementioned mechanism, we performed a time dependent starch digestion study employing UV–Vis spectroscopy. The protocol for this characterization has been elaborated in the Section (IV) of the ESI. The plots in the Fig. 3**(C)** show that the area under the curve for the SAuNP peak rapidly reduced with time due to the faster digestion of starch in presence of the AuNPs and Cl^- ions upon α-amylase addition. In comparison, the degradation of starch-iodine complex in absence AuNPs and Cl^- ions were found to be much slower, which was reflected in smaller reduction in the area under the curve with time corresponding to the starch-iodine peak, as shown in the Fig. 3**(D)**. It may be noted here that the increase in the activity of α-amylase due to presence of Cl^- ions is a well-established fact (Levitzki and Steer, 1974; Numao et al., 2002). The small sized Cl^- ions can easily fit into the cleft present in the enzyme, which brings in structural change resulting in the increased activity of the enzyme. In the similar lines, the Fig. 3**(c)** and

S1(C) of ESI corroborate that Cl^- ions helped in the faster starch digestion from SAuNP. Fig. 3**(E)** shows the energy-dispersive x-ray spectroscopy (EDXS) of the sensor, which confirmed the presence of Cl^- on surface. The starch digestion kinetics study based on the IR and UV–Vis spectroscopy together with EDXS suggested the presence of AuNPs and Cl^- ions were the major reasons behind, (i) the reduction in the electrical resistance with α-amylase loading and (ii) a smaller response time of sensor.

The plot in Fig. 3**(F)** shows the Raman spectroscopy of the sensor surface. The peak for gluconic acid at 1072 cm^{-1} (Al-Ogaidi et al., 2014; Kaminský et al., 2009) supports the conversion of glucose into gluconic acid during the reduction of Au^{3+} ions in $HAuCl_4$ into SAuNPs. Previous studies suggested that during the formation of the SAuNPs, the intrinsic electrical properties may change with time. (Zareh et al., 2011) In this direction, we characterized the electrical properties of the sensing materiel composed of polyaniline, AuNP, and starch. The experiments uncover that while PANI-ES-AuNP showed an electrical resistance of about 200 kΩ the PANI-ES-SAuNP showed about 440 MΩ. In this regard, we have provided a summary of the protocol for the optimization of starch and $HAuCl_4$ loading on the sensor in the Section (V) of the ESI. The variation in initial resistance of the sensor was ~1% over six months', as discussed with the Fig. S2 in the Section (VI) of the ESI.

2.4. Device proposition

The experimental setup shown in the Fig. 4 was employed for measuring the change in resistance of the biosensor with the concentration of the aqueous α-amylase solution. Fig. 4**(A)** shows the image of the sourcemeter, which measured the change in resistance. Figs. 4**(B)** and 4**(C)** show that the electrical contacts were made with a conductive silver paste. Fig. 4**(D)** depicts the change in normalized resistance (R/R_0) of the sensor with the variation in the α-amylase concentration (C). In the beginning of the experiments, the resistance of the PANI-ES film loaded with SAuNPs was evaluated as the base resistance R_0. The resistance (R) obtained after the addition of the aqueous α-amylase solution on the sensor was normalized with R_0 while plotting in Fig. 4**(D)**. It may be noted here that each experiment was repeated for five times and the deviation in the data was represented as the error bars in the Fig. 4**(D)**. Fig. S3 in the section (VII) of the ESI shows a linear variation in the normalized electrical resistance (R/R_0) with the concentration (C) in the range 30 U/L to 90 U/L with an R^2 value of ~0.99. This fit was found to be suitable for the preparation of the calibration plot in that range.

The normal level of α-amylase in blood serum is between 24 and 85 U/L, which was the basis for the chosen concentration range in Fig. 4**(D)**. (Nater et al., 2005; Wilkins, 2009) The figure shows that R/R_0 reduced when C increased in the droplet dispensed on the sensor. A larger α-amylase loading depleted larger amount of starch present on the SAuNPs, which led to the reduction in resistance of the sensor. The variation of R/R_0 with C was employed as the calibration plot to detect unknown quantities of α-amylase in human serum. The triangular symbols of Fig. 4**(D)** shows the results of the human serum samples alongside the calibration curve obtained. In this case, initially, we employed clinically approved samples and methodology involving the equipment Dimension RxL Max Integrated Chemistry System (SIEMENS), to obtain the activity of α-amylase in a sample of human serum (Chen et al., 2014; Fei et al., 2015). Thereafter, we dispensed the same sample to obtain the amount of α-amylase form the proposed sensor using the calibration plot. In this regard, we dispensed the serum directly on the sensor without any further treatment. Fig. 4**(D)** suggests that the α-amylase levels in the serum samples could be predicted accurately using the proposed sensor. The Table S2 in Section (VII) of the ESI shows the typical comparison of the unknown level of α-amylase in human serum measured by the proposed methodology with the clinically approved protocol. The table suggest that the predictions by the POCT device was rather close with some deviations as compared to the clinically approved methodology. The deviations obtained in the proposed POCT methodology as compared to the costly clinically approved method could be attributed to the optimization and improvement of the proposed biosensor. Importantly, the tests involving human serum were carried out under the supervision of medical experts in a nearby diagnostic centre.

Fig. 4**(E)** shows the working prototype of the proposed α-amylase sensor. The prototype was composed of a biosensor, a sample stage, a SPU with a built-in sourcemeter, and a LC-RTD. Fig. 4**(F)** illustrates the circuit diagram for the proposed POCT device in which the domain (i) corresponds to the open source microcontroller board, (ii) is the LC-RTD, and (iii) is the modified voltage divider circuit with the built-in sourcemeter to integrate the biosensor and microcontroller. The detailed description of the circuit is provided in the Section (VIII) of the ESI. The microcontroller unit of the POCT device was loaded with the calibration data to perform the tests with human serum while the built-in sourcemeter transferred the electrical resistance directly to the controller. The circular and square symbols in the Fig. 4**(D)** show that the POCT device was able to reproduce the electrical resistance of the biosensor obtained from the commercially available sourcemeter. Integration of this step helped in excluding the use of the commercial sourcemeter for resistance measurement, which in turn facilitated the lowering of the device cost and operation time as a POCT device.

A simple simulation shown in the Fig. S4 in the Section (IX) of the ESI helped in explaining the reduction in the resistance of the biosensor with the depletion of the starch loading on the AuNPs. In this figure, we consider two-dimensional (2-D) geometry of 5 μm width in which a starch film of thickness h loaded with AuNPs (dia. 100 nm) was resting on a PANI-ES film of thickness 0.5 μm. The Ampere's law was solved for the entire domain with the boundary conditions $V_a = 10$ mV at the zone of terminal metal contact, 0 V at the zone of grounded portion, and insulation boundary condition in the remaining places. The simulations suggested that resistance of the sensor decreased with reduction in the volume fraction (ϕ) of starch, which was obtained by evaluating the ratio of the area occupied solely by starch film to the total area occupied by the starch and AuNPs inside the starch layer. It is well known that starch has weak electrical conductivity and a thick layer of it is bound to increase the effective resistance of the sensor. However, with the increase in the dosage of α-amylase, the depletion of higher amount of starch on the sensor caused the reduction in the effective resistance of the sensor, which was observed both experimentally and computationally in the Fig. 4**(D)** and **S4**. Although the comparison between the experimental and computational results was rather qualitative, the reduction in the resistance with the increase (reduction) in the dosage (amount) of α-amylase (starch) was found to be monotonic and liner. A detailed computational investigation on the exact characteristics of the sensing mechanism is kept as a future scope of research.

3. Conclusions

We report the fabrication of a simple, rapid, reliable, and economic POCT device for the detection of α-amylase enzyme in human serum. The device is composed of an electrical biosensor, a sample stage, a signal processing unit with a built in sourcemeter, and a real time display. The biosensor is composed of an electrically conducting PANI-ES thin film covered with starch-coated gold nanoparticles (SAuNPs). Experiments uncovered the pathways to SAuNP formation on PANI-ES, time-dependent starch digestion on the same with α-amylase loading, and the subsequent variation in electrical response. Presence of AuNPs and Cl^- ions on the biosensor surface helped in a rapid starch hydrolysis with α-amylase while the use of the conducting polymer film as substrate provided stability in obtaining the electronic signals.

The reduction in the resistance with the increase (reduction) in the dosage (amount) of α-amylase (starch) was monotonic and liner, which helped in calibrating the microcontroller unit. Since we employed a

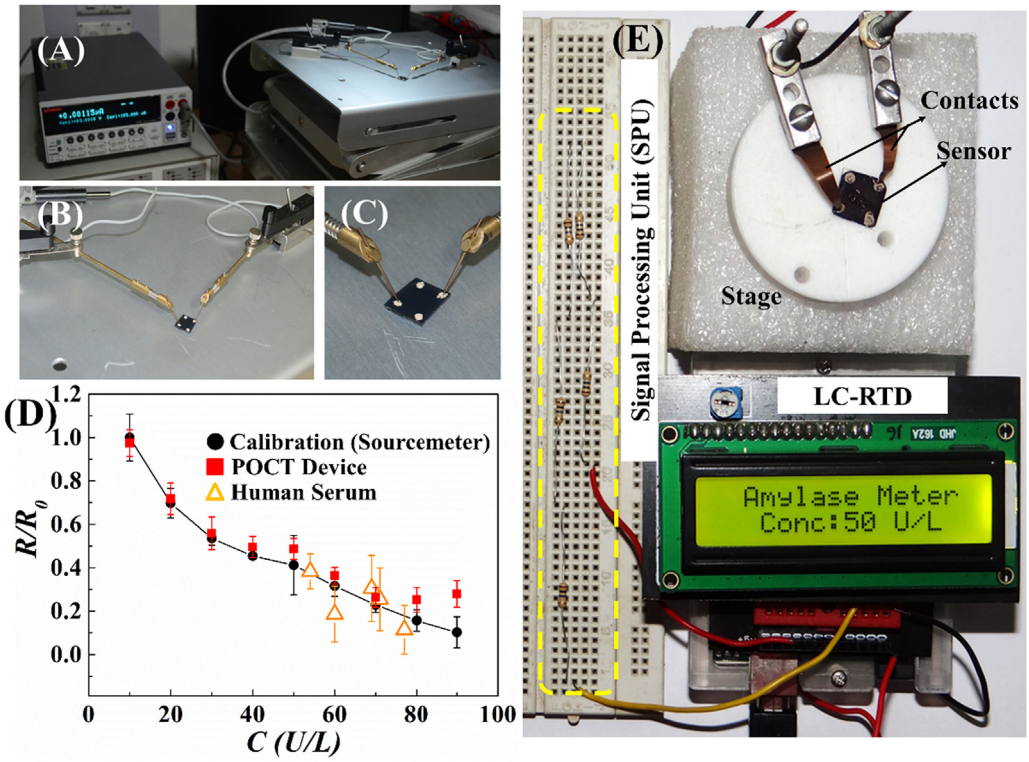

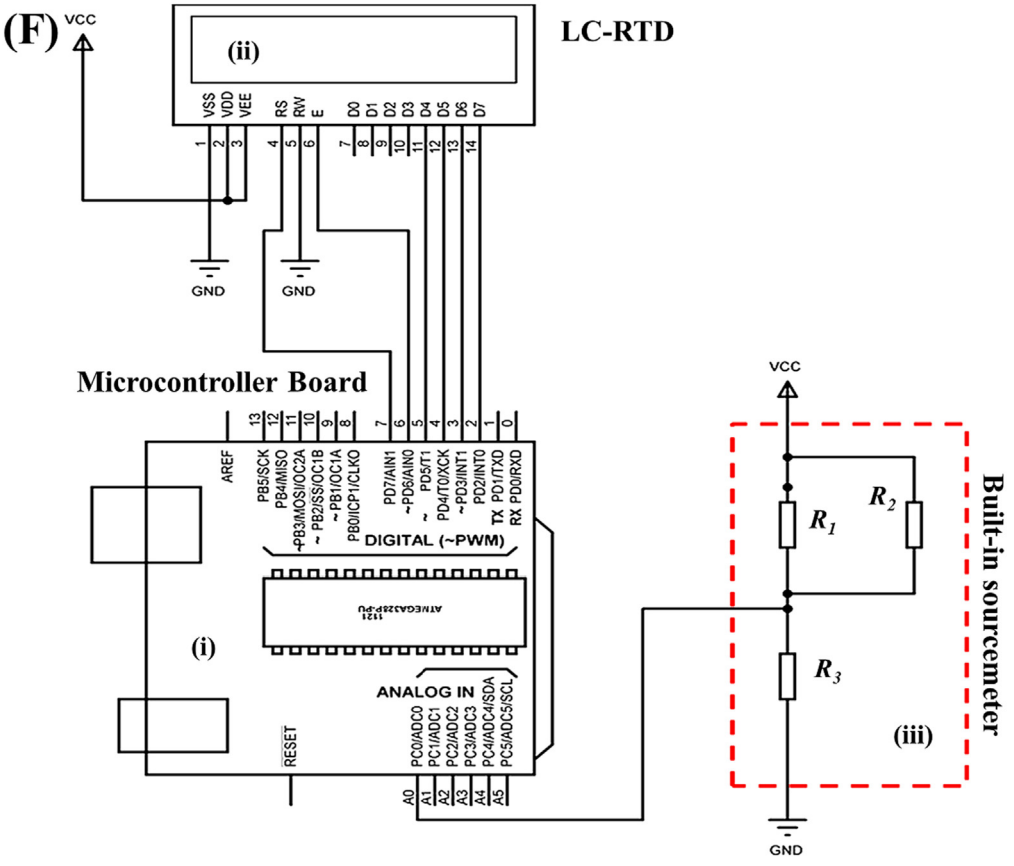

Fig. 4. The image (A) shows the commercial sourcemeter for resistance measurement and the image (B) shows the silver paste electrical contacts on the sensor, which is magnified in image (C). The image (D) shows the variation in the normalized resistance (R/R_0) with α-amylase concentration in the analyte (C). The image shows the calibration plot using the commercially available sourcemeter (circular symbols) using α-amylase solution prepared in the laboratory, the same data reproduced by the POCT device (square symbols), and the test data measured by the POCT device using human serum of unknown level of α-amylase (triangular symbols). Image (E) shows the photograph of the POCT device composed of a sensor, a sample stage, a signal processing unit (SPU) with a built-in sourcemeter, and a liquid-crystal-real-time-display (LC-RTD). The image (F) illustrates the circuit diagram of the POCT device where, (i) corresponds to microcontroller board, (ii) LC-RTD, and (iii) voltage divider circuit with the built-in sourcemeter.

very selective and specific bio-reaction – starch hydrolysis by α-amylase, the POCT device was equally efficient in detecting the unknown level of α-amylase in human serum. The accuracy of the POCT device compared and contrasted with a clinically approved method. Integration of the built-in sourcemeter facilitated *in situ* measurement of electrical resistance, excluding the necessity of a commercial sourcemeter.

The proposed POCT device can be employed for the immediate detection of α-amylase in human serum, which helps in the diagnosis of pancreatitis, cancer, mumps, stress, and depression. With some simple

modifications, the device can also be employed to detect α-amylase in serum, saliva, or sebum, which is kept as a future scope of research work.

Supporting information

The materials, methods, FTIR and UV–Vis spectroscopy, a brief detail of the PCB circuit, and the computational methodology are provided along with this article.

Acknowledgements

We thank Ministry of Electronics and Information Technology (MeitY) 5(9)/2012-NANO and Department of Science and Technology-Fund for Improvement of S&T infrastructure in universities & higher educational institutions (DST-FIST) grant no. SR/FST/ETII-028/2010, Government of India, for financial aids. We thank the support from CIF, IIT Guwahati for characterization facilities. Discussions with Amit, Anushree, and Srestha are also acknowledged.

Author information

Nilanjan Mandal and Dipankar Bandyopadhyay designed the experimental and computational studies. Nilanjan Mandal performed the experimental and computational investigations. Mitradip Bhattacharjee helped in designing the electronic circuit. The manuscript was written through contributions from all authors and they have given approval to the final version. The authors declare no conflict of interest.

Appendix A. Supporting information

Supplementary data associated with this article can be found in the online version at doi:10.1016/j.bios.2018.09.097.

References

Ahn, C.H., Jin-Woo, C., Beaucage, G., Nevin, J.H., Jeong-Bong, L., Puntambekar, A., Lee, J.Y., 2004. Proceedings of the IEEE 92 (1), 154–173.
Al-Ogaidi, I., Gou, H., Al-kazaz, A.K.A., Aguilar, Z.P., Melconian, A.K., Zheng, P., Wu, N., 2014. Anal. Chim. Acta 811, 76–80.
Anderson, K.L., 2002. Anaerobe 8 (5), 269–276.
Bandyopadhyay, D., Mandal, N., Dutta, S., 2016. Indian Patent Application No: 201731032122 A.
Bashir, R., 2004. 56(11), 1565–1586.
Battershell, V.G., Henry, R.J., 1990. J. Cereal Sci. 12 (1), 73–81.
Bernfeld, P., 1955. Amylases, α and β. In: Colowick, S.P., Kaplan, N.O. (Eds.), Methods in Enzymology. Academic Press, pp. 149–158.
Bhattacharjee, M., Pasumarthi, V., Chaudhuri, J., Singh, A.K., Nemade, H., Bandyopadhyay, D., 2016. Nanoscale 8 (11), 6118–6128.
Bhattacharjee, M., Nemade, H.B., Bandyopadhyay, D., 2017. 94, pp. 544-551.
Bhattacharya, S., Jang, J., Yang, L., Akin, D., Bashir, R., 2007. J. Rapid Methods Autom. Microbiol. 15 (1), 1–32.
Castillo-López, D.N., Pal, U., 2014. J. Nanopart. Res. 16 (8), 2571.
Chairam, S., Poolperm, C., Somsook, E., 2009. Carbohydr. Polym. 75 (4), 694–704.
Chavez, R.G., David, H., Metzner, E.K., Sigler, G.F., Winn-Deen, E.S., 1990. US Patent No. 4963479A.
Chen, Y.-C., Chiou, C., Lin, M.-N., Lin, C.-L., 2014. PLoS One 9 (12), e115145.
Chin, C.D., Linder, V., Sia, S.K., 2007. Lab Chip 7 (1), 41–57.
Cosnier, S., 1999. Biosens. Bioelectron. 14 (5), 443–456.
Deka, J., Paul, A., Ramesh, A., Chattopadhyay, A., 2008. Langmuir 24 (18), 9945–9951.
Dutta, S., Mandal, N., Bandyopadhyay, D., 2016. Biosens. Bioelectron. 78, 447–453.
Engelbrekt, C., Sorensen, K.H., Zhang, J., Welinder, A.C., Jensen, P.S., Ulstrup, J., 2009. J. Mater. Chem. 19 (42), 7839–7847.
Engelbrekt, C., Jensen, P.S., Sørensen, K.H., Ulstrup, J., Zhang, J., 2013. J. Phys. Chem. C 117 (22), 11818–11828.
Fei, K., Xiangshu, H., Kun, X., 2015. Nanotechnology 26 (40), 405707–405715.
Ferrari, M., Bashir, R., Wereley, S., 2006. BioMEMS and Biomedical Nanotechnology. Springer US, pp. 93–115.
Foo, A.Y., Bais, R., 1998. Clin. Chim. Acta 272 (2), 137–147.
Gibbs, M.J., Biela, A., Krause, S., 2015. Biosens. Bioelectron. 67, 540–545.
Gogoi, S.K., Borah, S.M., Dey, K.K., Paul, A., Chattopadhyay, A., 2011. Langmuir 27 (20), 12263–12269.
Gogoi, S.K., Paul, A., Chattopadhyay, A., 2012. RSC Adv. 2 (9), 3642–3646.
González, C.F., Fariña, J.I., Figueroa, L.I.C., 2002. Enzym. Microb. Technol. 30 (2), 169–175.
Grieshaber, D., MacKenzie, R., Vörös, J., Reimhult, E., 2008. Sensors 8 (3), 1400–1458.
Han, J., Li, L., Guo, R., 2010. Macromolecules 43 (24), 10636–10644.
He, D., Cai, Y., Wei, W., Nie, L., Yao, S., 2000. Biochem. Eng. J. 6 (1), 7–11.
Homola, J., 2008. Chem. Rev. 108 (2), 462–493.
Imberty, A., Chanzy, H., Pérez, S., Bulèon, A., Tran, V., 1988. J. Mol. Biol. 201 (2), 365–378.
Janowitz, H.D., Dreiling, D.A., 1959. Am. J. Med. 27 (6), 924–935.
Jenkins, P.J., Donald, A.M., 1995. Int. J. Biol. Macromol. 17 (6), 315–321.
Kaminský, J., Kapitán, J., Baumruk, V., Bednárová, L., Bouř, P., 2009. J. Phys. Chem. A 113 (15), 3594–3601.
Katti, K.K., Kattumuri, V., Bhaskaran, S., Katti, K.V., Kannan, R., 2009. Int. J. Green Nanotechnol. Biomed. 1 (1), B53–B59.
Kricka, L.J., 2001. Clin. Chim. Acta 307 (1–2), 219–223.
Kricka, L.J., Nozaki, O., Heyner, S., Garside, W.T., Wilding, P., 1993. Clin. Chem. 39 (9), 1944–1947.
Levitzki, A., Steer, M.L., 1974. Eur. J. Biochem. 41 (1), 171–180.
Li, D., Kaner, R.B., 2005. J. Am. Chem. Soc. 128 (3), 968–975.
Mahosenaho, M., Caprio, F., Micheli, L., Sesay, A., Palleschi, G., Virtanen, V., 2010. Microchim. Acta 170 (3–4), 243–249.
Malhotra, B.D., 2001. Handbook of Polymers in Electronics, First ed. Rapra Technology Limited, UK, pp. 393–423.
Mallick, K., Witcomb, M., Scurrell, M., 2006. Gold. Bull. 39 (4), 166–174.
Manz, A., Graber, N., Widmer, H.M., 1990. Actuators B 1 (1–6), 244–248.
Murayama, T., Tanabe, T., Ikeda, H., Ueno, A., 2006. Bioorg. Med. Chem. 14 (11), 3691–3696.
Nater, U.M., Rohleder, N., Gaab, J., Berger, S., Jud, A., Kirschbaum, C., Ehlert, U., 2005. Int J. Psychophysiol. 55 (3), 333–342.
Numao, S., Maurus, R., Sidhu, G., Wang, Y., Overall, C.M., Brayer, G.D., Withers, S.G., 2002. Biochemistry 41 (1), 215–225.
Pandey, P.C., Mishra, A.P., 1988. Analyst 113 (2), 329–331.
Pasta, M., La Mantia, F., Cui, Y., 2010. Electrochim. Acta 55 (20), 5561–5568.
Pillalamarri, S.K., Blum, F.D., Tokuhiro, A.T., Bertino, M.F., 2005. Chem. Mater. 17 (24), 5941–5944.
Raveendran, P., Fu, J., Wallen, S.L., 2003. J. Am. Chem. Soc. 125 (46), 13940–13941.
Robles, T.F., Shetty, V., Zigler, C.M., Glover, D.A., Elashoff, D., Murphy, D., Yamaguchi, M., 2011. Biol. Psychol. 86 (1), 50–56.
Saliterman, S., 2006. Fundamentals of BioMEMS and Medical Microdevices, First ed. Wiley, USA, pp. 413–448.
Sarma, T.K., Chattopadhyay, A., 2004. Langmuir 20 (11), 4733–4737.
Sasaki, T., Noel, T.R., Ring, S.G., 2008. J. Agric. Food Chem. 56 (3), 1091–1096.
Shetty, V., Zigler, C., Robles, T.F., Elashoff, D., Yamaguchi, M., 2011. Psychoneuroendocrinology 36 (2), 193–199.
Sia, S.K., Kricka, L.J., 2008. Lab Chip 8 (12), 1982–1983.
Singh, A.K., Dey, K.K., Chattopadhyay, A., Mandal, T.K., Bandyopadhyay, D., 2014. Nanoscale 6 (3), 1398–1405.
Singh, S., Solanki, P.R., Pandey, M.K., Malhotra, B.D., 2006. Sens. Actuators B 115 (1), 534–541.
Sky-Peck, H., Thuvasethakul, P., 1977. Ann. Clin. Lab. Sci. 7 (4), 310–317.
Snabe, T., Petersen, S.B., 2002. J. Biotechnol. 95 (2), 145–155.
Svens, E., Käpyaho, K., Tanner, P., Weber, T.H., 1989. Clin. Chem. 35 (4), 662–664.
Swaroop, V., Chari, S.T., Clain, J.E., 2004. J. Am. Med. Assoc. 291 (23), 2865–2868.
Tahir, Z.M., Alocilja, E.C., Grooms, D.L., 2005. Biosens. Bioelectron. 20 (8), 1690–1695.
Tajammul Hussain, S., Iqbal, M., Mazhar, M., 2008. J. Nanopart. Res. 11 (6), 1383.
Takeuchi, T., Matsushima, T., Sugimura, T., 1975. Clin. Chim. Acta 60 (2), 207–213.
Tamer, U., Seçkin, A.İ., Temur, E., Torul, H., 2011. Int. J. Electrochem. 2011, 1–7.
Trojanowicz, M., Krawczyński vel Krawczyk, T., 1995. Microchim. Acta 121 (1–4), 167–181.
van Staden, J.F., Mulaudzi, L.V., 2000. Anal. Chim. Acta 421 (1), 19–25.
Vo-Dinh, T., Cullum, B., 2000. Fresenius J. Anal. Chem. 366 (6–7), 540–551.
Walker, G.J., Hope, P.M., 1963. Biochem. J. 86 (3), 452–462.
Wang, H., Mu, S., 1999. Sens. Actuators B 56 (1–2), 22–30.
Wang, J., Neoh, K.G., Kang, E.T., 2001. J. Colloid Interface Sci. 239 (1), 78–86.
Wang, S., Copeland, L., 2015. Crit. Rev. Food Sci. Nutr. 55 (8), 1081–1097.
Wang, Y.-J., Truong, V.-D., Wang, L., 2003. Carbohydr. Polym. 52 (3), 327–333.
Warshaw, A.L., Fuller, A.F., 1975. N. Engl. J. Med. 292 (7), 325–328.
Watanabe, T., Yamamoto, A., Nagai, S., Terabe, S., 1998. Electrophoresis 19 (13), 2331–2337.
Whitesides, G.M., 2006. Nature 442 (7101), 368–373.
Wilkins, L.W., 2009. Diagnostic Tests Made Incredibly Easy!, Second ed. Lippincott Williams & Wilkins, pp. 29–252.
Wu, C., Brunelle, F., Harnois, M., Follet, J., Senez, V., 2012. Micro Electro Mechanical Systems (MEMS), In: IEEE Proceedings of the 25th International Conference on, pp. 777–780.
Yager, P., Edwards, T., Fu, E., Helton, K., Nelson, K., Tam, M.R., Weigl, B.H., 2006. Nature 442 (7101), 412–418.
Yager, P., Domingo, G.J., Gerdes, J., 2008. Annu. Rev. Biomed. Eng. 10 (1), 107–144.
Yamaguchi, M., Deguchi, M., Wakasugi, J., 2005. Biomed. Micro. 7 (4), 295–300.
Zajoncová, L., Jílek, M., Beranová, V., Peč, P., 2004. Biosens. Bioelectron. 20 (2), 240–245.
Zareh, E.N., Moghadam, P.N., Azariyan, E., Sharifian, I., 2011. Iran. Polym. J. 20 (4), 319–328.
Zhang, Z., Seitz, W.R., O'Connell, K., 1990. Anal. Chim. Acta 236, 251–256.